Tunable plasmonic dichroism of Au nanoparticles self-aligned on rippled Al_2O_3 thin films

A Letters Journal Exploring the Frontiers of Physics

January 2011

EPL, **93** (2011) 26005
doi: 10.1209/0295-5075/93/26005

www.epljournal.org

Tunable plasmonic dichroism of Au nanoparticles self-aligned on rippled Al_2O_3 thin films

D. Babonneau[1(a)], S. Camelio[1], L. Simonot[1], F. Pailloux[1], P. Guérin[1], B. Lamongie[1] and O. Lyon[2]

[1] *Institut Pprime, Département Physique et Mécanique des Matériaux, UPR 3346 CNRS, Université de Poitiers, SP2MI, Téléport 2 - Bvd. M. et P. Curie, BP 30179, 86962 Futuroscope Chasseneuil Cedex, France, EU*
[2] *Synchrotron SOLEIL, L'Orme des Merisiers Saint-Aubin - BP 48, 91192 Gif-sur-Yvette, France, EU*

received 9 December 2010; accepted in final form 14 January 2011
published online 7 February 2011

PACS 61.46.-w – Structure of nanoscale materials
PACS 78.67.-n – Optical properties of low-dimensional, mesoscopic, and nanoscale materials and structures
PACS 81.16.-c – Methods of micro- and nanofabrication and processing

Abstract – The self-alignment and optical dichroism of Au nanoparticle chains grown by glancing incidence deposition on rippled Al_2O_3 thin films is investigated. Although the nucleation of the nanoparticles is almost isotropic, their growth is strongly anisotropic resulting in a sharp dependence of their optical transmittance on the orientation of the polarization of the incident light. We show that both the frequency and the spectral width of the transverse and longitudinal surface plasmon resonances can be easily tuned by varying the amount of deposited metal. Such nanostructured materials open perspectives for the development of plasmonic devices endowed with tunable optical dichroism both in the visible and the near infrared regimes.

Introduction. – Planar arrays of metallic nanostructures such as nanoparticles or nanowires periodically aligned on dielectric surfaces are ideal for fundamental studies of coupling and ordering phenomena as well as for applied research on plasmonics [1], photovoltaics [2], and magnetism [3]. Especially, noble metal nanostructures have received considerable attention lately due to a range of possible applications as dichroic filters, molecular sensors, and subwavelength photonic waveguides exploiting the selective photon absorption and local field enhancement arising at wavelengths near the so-called surface plasmon resonance (SPR) condition [4]. Despite the progress in nanofabrication techniques, the realization of nanostructures with well-controled composition, size, shape, and distribution remains a significant challenge, especially for the large-scale production of regular arrays on substrates that may be applied as dichroic filters [5–7]. Lithographic techniques could potentially offer a solution [8,9], but are not suitable for most practical purposes owing to the low output and high production costs. Recent advances in nanostructure preparation using colloidal chemistry show that self-alignment of metallic nanorods may be realized, providing an easy and inexpensive way for tailoring the plasmonic properties of metamaterials [10–13]. Another effective and low-cost method to fabricate large-area arrays of Au and Ag nanostructures consists in combining substrate prepatterning by defocused ion-etching with subsequent Volmer-Weber growth by physical vapor deposition at glancing angles [14–17]. It has been proved that these materials possess promising optical properties due to their morphological anisotropy reflected in a sharp polarization-dependent excitation of their localized surface plasmons. The ability to tune the optical dichroism of Au [15] and Ag [17] nanowires by varying the amount of deposited metal (t_{metal}) has been proved recently. However, there is still no report on the influence of t_{metal} on the growth mechanisms as well as the resulting optical properties in the low metal-coverage regime (*i.e.*, when disconnected nanoparticles are formed). In this article, we demonstrate that the optical dichroism of Au nanoparticle arrays grown on rippled alumina thin films can be easily tuned either in the visible ($t_{\mathrm{Au}} \leqslant 1\,\mathrm{nm}$) or both in the visible and the near infrared regime ($t_{\mathrm{Au}} \geqslant 2\,\mathrm{nm}$). The relationship between such optical properties and the structure (morphology and organization) of the nanoparticles is discussed.

(a) E-mail: david.babonneau@univ-poitiers.fr

Experimental. – Rippled surfaces were produced on 90 nm thick amorphous Al_2O_3 thin films deposited by ion-beam sputtering onto fused-silica substrates and carbon-coated copper grids. Ion-etching was performed at room temperature with Xe^+ ions at a sputtering angle of $\theta = 55°$ with respect to the surface normal, with an ion energy $E = 1000$ eV, and a fluence of about 3.6×10^{16} ions cm^{-2} (ion flux $\sim 2 \times 10^{14}$ ions cm^{-2} s^{-1}), leading to ripples that are oriented perpendicular to the ion beam [16]. The rippled thin films were used as templates with the aim of creating self-organized chains of Au nanoparticles. Deposition of Au was accomplished at a temperature of 200 °C and a rate of 0.01 nm s^{-1} by DC magnetron sputtering under a glancing incidence of 5° from the surface, with the atomic flux being oriented opposite to the Xe^+ beam. The effective Au thickness was varied between $t_{Au} = 0.5$ nm and $t_{Au} = 3.0$ nm in order to avoid the formation of Au nanowires. The rippled thin films before and after Au deposition were examined by grazing incidence small-angle X-ray scattering (GISAXS) on the SWING beamline at SOLEIL synchrotron with different orientations of the incident X-ray beam with respect to the ripples. The energy of the incident X-ray beam was 11.857 keV, the angle of incidence was $\alpha_i = 0.3°$, and the scattered photons were collected as a function of the in-plane $2\theta_f$ and out-of-plane α_f exit angles with a two-dimensional CCD detector (fig. 1(a)). The planar arrays of Au nanoparticles were also characterized by high-angle annular dark-field scanning transmission electronic microscopy (HAADF-STEM) with a JEOL 2200FS microscope using an acceleration voltage of 200 kV, a probe size of 0.7 nm, and an inner collection angle of 50 mrad. The optical properties were investigated by means of spectroscopic transmission of polarized light in the range between 400 and 950 nm by using a QE65000 Ocean Optics^{TM} spectrophotometer.

Results. – Figure 1(b) shows the GISAXS pattern of an as-etched Al_2O_3 thin film recorded with the incident X-ray beam along the x-direction perpendicular to the Xe^+ beam. Two vertical streaks on either side of the z-axis are readily observed, indicating a periodic surface corrugation (namely ripples) with a wave vector along the y-direction parallel to the Xe^+ beam. The position and width of the streaks are related to the period L_y and correlation length ξ_y of the surface corrugation, while the vertical extend of the streaks is related to the ripple height h [16]. The quantitative analysis of the GISAXS intensity was performed in the framework of the distorted-wave Born approximation with the *FitGISAXS* program [18] assuming a rippled surface with a symmetric sawtooth profile as shown in fig. 1(c) where $\tan\gamma = 2h/L_y$. The full GISAXS map was fitted within the local monodisperse approximation by using the one-dimensional paracrystal model [19] to retrieve L_y and ξ_y, and by assuming a log-normal distribution of L_y with a mean period $\langle L \rangle = L_y \exp[\frac{3}{2}(\ln\sigma)^2]$, and a dispersion $\ln\sigma$.

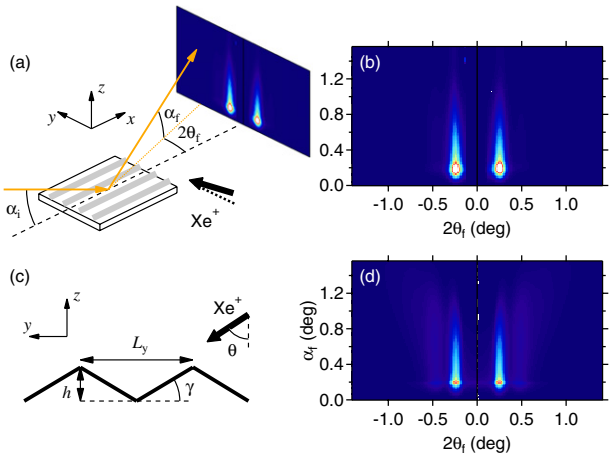

Fig. 1: (Colour on-line) (a) Schematic drawing of the GISAXS geometry. (b) Experimental GISAXS pattern of a rippled Al_2O_3 thin film with the incident X-ray beam along the x-direction. (c) Schematic drawing of the model surface profile. (d) Simulated GISAXS pattern with the parameters obtained from the fit of the experimental map.

Figure 1(d) exhibits the result of the fit obtained from the experimental data displayed in fig. 1(b) thus providing $L_y = 23.5$ nm, $\xi_y = 1930$ nm, $\ln\sigma = 0.15$, and $\gamma = 31.9°$.

Figures 2(a)–(c) show the plane-view HAADF-STEM images and corresponding autocorrelation functions of similar rippled Al_2O_3 thin films after glancing-angle Au deposition, with effective thicknesses of $t_{Au} = 0.5$ nm, 1.0 nm, and 3.0 nm, respectively. Our observations indicate that despite shadowing effects, the initial stages of Au growth (fig. 2(a)) is characterized by an almost isotropic nucleation owing to the high surface diffusivity of Au on Al_2O_3 at 200 °C. In contrast, at higher coverage rates (figs. 2(b) and (c)), the in-plane distribution of the Au nanoparticles becomes strongly anisotropic with short-range order in the x-direction and long-range order in the y-direction. Moreover, the period of the chains of nanoparticles corresponds to that of the ripples, L_y, suggesting that the periodicity is imposed by the prepatterned Al_2O_3 template [14–17]. The in-plane size and shape distributions of the Au nanoparticles were analyzed from the plane-view HAADF-STEM images by assuming hemiellipsoids with in-plane projected sizes D_x and D_y along the x- and y-directions, respectively. The mean values $\langle D_x \rangle$ and $\langle D_y \rangle$ together with the corresponding standard deviations σ_x and σ_y are reported in table 1. It is worth noting that not only the effective in-plane size $D = \sqrt{\langle D_x \rangle \langle D_y \rangle}$, but also the shape anisotropy of the nanoparticles ($\langle D_x \rangle / \langle D_y \rangle$) increase with t_{Au}. Actually, for $t_{Au} = 3.0$ nm, agglomeration and coarsening proceed leading to the formation of elongated nanoparticles predominantly aligned along the direction of the ripples (*i.e.*, perpendicular to the Au atomic flux). Furthermore, it is worth noting that whereas the size dispersion in the y-direction ($\sigma_y / \langle D_y \rangle$) tends to reach a saturation value

Table 1: Structural parameters retrieved from HAADF-STEM and GISAXS analyses as a function of the Au effective thickness t_{Au}. In-plane mean projected sizes $\langle D_x \rangle$ and $\langle D_y \rangle$ and corresponding standard deviations σ_x and σ_y (from HAADF-STEM). Out-of-plane sizes of the nanoparticles H, interparticle distances L_x, and corresponding correlation length ratios ξ_y/ξ_x (from GISAXS).

t_{Au} (nm)	$\langle D_x \rangle$ (nm)	σ_x (nm)	$\sigma_x/\langle D_x \rangle$	$\langle D_y \rangle$ (nm)	σ_y (nm)	$\sigma_y/\langle D_y \rangle$	H (nm)	L_x (nm)	ξ_y/ξ_x
0.5	3.8(5)	1.6(4)	0.4(3)	3.5(9)	1.4(3)	0.4(0)	2.7(8)	5.5(4)	18.8
1.0	7.3(9)	5.2(7)	0.7(1)	6.8(5)	4.2(0)	0.6(1)	4.6(3)	9.4(8)	10.8
3.0	17.9(6)	17.2(2)	0.9(6)	11.9(6)	7.2(6)	0.6(1)	8.8(0)	18.4(6)	4.25

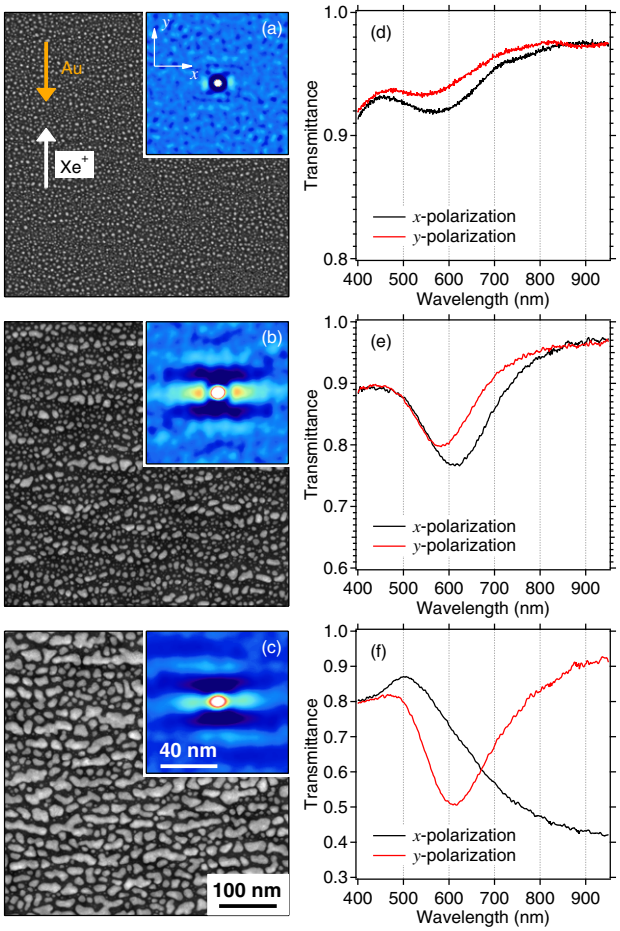

Fig. 2: (Colour on-line) Plane-view HAADF-STEM images of rippled Al_2O_3 thin films after glancing-angle Au deposition. The effective Au thicknesses are (a) $t_{\mathrm{Au}} = 0.5$ nm, (b) $t_{\mathrm{Au}} = 1.0$ nm, and (c) $t_{\mathrm{Au}} = 3.0$ nm. The directions of the Xe^+ beam and Au flux are indicated by the arrows, and the autocorrelation functions of the images are shown in the insets. (d–f) Corresponding transmission measurements at normal incidence with the polarization of the incoming light being oriented parallel (x-polarization) and perpendicular (y-polarization) to the ripples.

of ~ 0.6 with increasing t_{Au}, the size distribution in the x-direction ($\sigma_x/\langle D_x \rangle$) dramatically broadens.

As seen in figs. 2(d)–(f), the structural anisotropy of such planar arrays of Au nanoparticles results in a dependence of their optical transmittance on the polarization of the incident light. For y-polarization (transverse excitation), the transmittance T_y shows a localized SPR whose spectral position changes from 540 nm to 610 nm when t_{Au} increases from 0.5 nm (fig. 2(d)) to 3.0 nm (fig. 2(f)). This behavior is characteristic of disconnected noble-metal islands supported on dielectric films and the spectral shift can be ascribed to a decrease of the effective out-of-plane ratio of the nanoparticles defined by H/D [20]. In addition, a progressive decrease of the transmittance minimum is readily observed, which is due to the increase of the nanoparticle volume and of the surface coverage. For x-polarization (longitudinal excitation), the transmittance T_x still shows a localized minimum when $t_{\mathrm{Au}} = 0.5$ nm and $t_{\mathrm{Au}} = 1.0$ nm. However, rotating the polarization from transverse to longitudinal results in a slight broadening of the SPR band together with a red-shift by approximately 30 nm, which cause an optical dichroism in the visible range only (fig. 3). For $t_{\mathrm{Au}} = 3.0$ nm, although the nanoparticles are still disconnected, the longitudinal transmittance T_x displays a spectral behavior characteristic of infinite metal nanowires, with a strong decrease toward the near infrared region and no evidence of localized SPR [21,22]. The resulting optical dichroism of the nanocomposite films is evidenced in fig. 3, which exhibits the difference in transmission $\Delta T = T_y - T_x$ divided by the transmittance T_y measured with transverse excitation. It appears that at high coverage ($t_{\mathrm{Au}} \geqslant 2$ nm), depending on the polarization, an efficient harvesting of

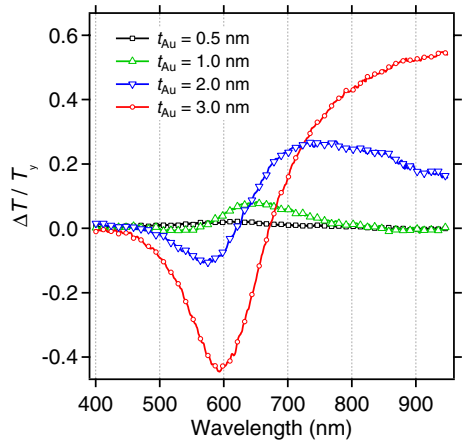

Fig. 3: (Colour on-line) Difference in transverse and longitudinal transmittances $\Delta T = T_y - T_x$ divided by the transverse transmittance T_y with increasing effective thicknesses from $t_{\mathrm{Au}} = 0.5$ nm to $t_{\mathrm{Au}} = 3.0$ nm.

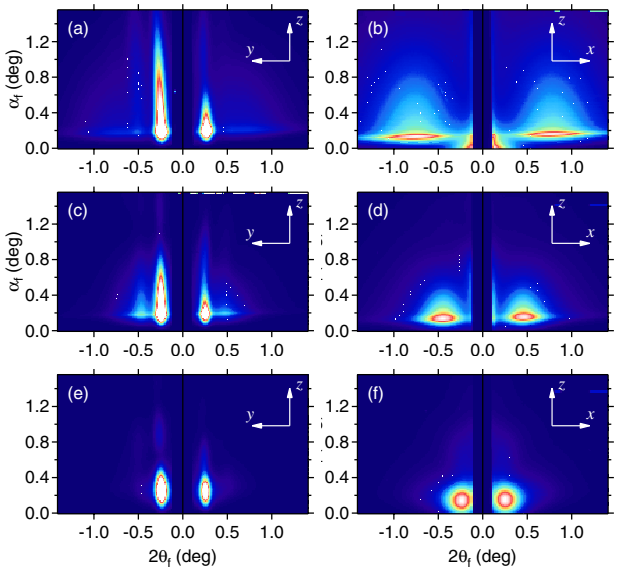

Fig. 4: (Colour on-line) Experimental GISAXS patterns of rippled Al_2O_3 thin films after glancing-angle Au deposition. (a) $t_{Au} = 0.5$ nm and X-rays along the x-direction, (b) $t_{Au} = 0.5$ nm and X-rays along the y-direction, (c) $t_{Au} = 1.0$ nm and X-rays along the x-direction, (d) $t_{Au} = 1.0$ nm and X-rays along the y-direction, (e) $t_{Au} = 3.0$ nm and X-rays along the x-direction, (f) $t_{Au} = 3.0$ nm and X-rays along the y-direction.

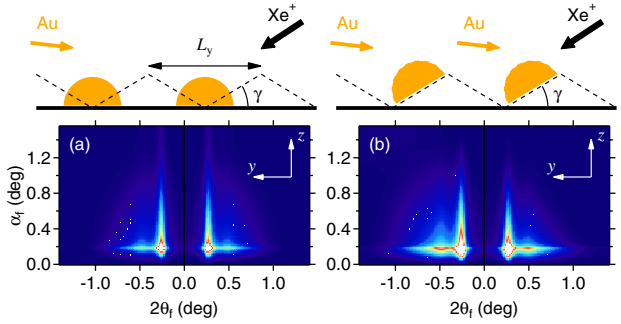

Fig. 5: (Colour on-line) Simulated GISAXS patterns ($t_{Au} = 1.0$ nm and X-rays along the x-direction) by assuming that the Au nanoparticles are (a) in the ripple valleys and (b) tilted from the surface normal by a tilt angle of γ.

light over a broadband spectrum [23] might be achieved either in the visible (y-polarization) or in the near infrared regime (x-polarization).

To go further in the structural characterization of the Au nanoparticles, figs. 4(a) and (b) show the GISAXS patterns of the nanocomposite film with $t_{Au} = 0.5$ nm recorded with the incident X-ray beam along the directions parallel (x-direction) and perpendicular (y-direction) to the ripples. In contrast to the HAADF-STEM observations (fig. 2(a)), the GISAXS measurements reveal a strong structural anisotropy. While the GISAXS pattern obtained with the X-ray beam along the y-direction exhibits two broad lobes expected for a planar distribution of nanoparticles with short-range order, the GISAXS pattern obtained with the X-ray beam along the x-direction displays intense and sharp streaks located at a position in excellent agreement with the corresponding GISAXS pattern before Au deposition (fig. 1(b)). However, it can be seen that the intensity distribution becomes strongly asymmetric after Au deposition, thus demonstrating that the scattering of the Au nanoparticles dominates the total GISAXS intensity as expected from the high contrast of electron density between Au and vacuum. It should be noticed that GISAXS patterns with similar characteristics were obtained with $t_{Au} = 1.0$ nm (figs. 4(c) and (d)) and $t_{Au} = 3.0$ nm (figs. 4(e) and (f)), with the scattered intensity concentrating toward the origin of the reciprocal space owing to the growth of the nanoparticles. The GISAXS patterns were analyzed assuming chains of hemiellipsoidal nanoparticles with in-plane dimensions $\langle D_x \rangle$ and $\langle D_y \rangle$, as determined from HAADF-STEM (table 1). Also, it has been considered that the distance between chains is L_y and the correlation length is ξ_y as extracted by GISAXS from as-etched Al_2O_3 thin films. First, the GISAXS maps recorded with the incident X-ray beam along the y-direction were fitted to determine the out-of-plane dimension H of the nanoparticles as well as the interparticle distance L_x and the corresponding correlation length ξ_x. The results reported in table 1 confirm that the effective out-of-plane ratio of the nanoparticles H/D decreases with t_{Au}, while the interparticle distance L_x increases progressively. Furthermore, in agreement with the HAADF-STEM analyses, it appears that the ξ_x values are much smaller than the corresponding ξ_y values. Also, it can be seen that the proximity of the nanoparticles in the x-direction is strongly affected, with the dimensionless parameter $\langle D_x \rangle / L_x$ increasing from 0.69 to 0.97. In contrast, $\langle D_y \rangle / L_y$ which increases from 0.15 to 0.51 is always smaller than 2/3, the value above which interparticle coupling effects become meaningful [24]. It is thus tempting to ascribe the red-shift of the longitudinal SPR to the increase of both the in-plane shape anisotropy and of the interparticle coupling effects, and its broadening to the strong increase of the dispersions of particle size and separation in the x-direction.

Finally, the parameters obtained previously were used to calculate the GISAXS intensity with the incident X-ray beam along the x-direction. Neglecting the ripple scattering and assuming the Au nanoparticles to be in the ripple valleys leads to a symmetric GISAXS pattern (fig. 5(a)), which is in disagreement with the experimental results. However, by considering nanoparticles tilted from the surface normal by a tilt angle of γ, the asymmetry of the experimental GISAXS map is well reproduced (fig. 5(b)). These results indicate that, although the planar distribution is almost isotropic at low coverage rates, a number of Au nanoparticles nucleate and then grow preferentially on the slopes of the rippled surface illuminated by the Au atomic flux during glancing-angle deposition, thus leading to a replication of the long-range order between ripples in the y-direction at higher coverage rates.

Conclusion. – In conclusion, we have presented evidence for the production of arrays of aligned Au nanoparticles using glancing-angle deposition on self-organized rippled Al_2O_3 templates. HAADF-STEM and GISAXS experiments combined with quantitative analysis provide complementary information on the influence of the shadowing effects on the growth mechanisms. We showed that the (in-plane and out-of-plane) shape anisotropy of the nanoparticles and their proximity to each other can be modified by varying the amount of deposited metal, which allows a dichroic and tunable optical response due to the anisotropic excitation of localized plasmons. For low Au coverage ($t_{\mathrm{Au}} \leqslant 1\,\mathrm{nm}$), almost isotropic nucleation and growth of the nanoparticles lead to the achievement of a weak optical dichroism in the visible range. For high Au coverage ($t_{\mathrm{Au}} \geqslant 2\,\mathrm{nm}$) and longitudinal excitation, these nanostructured materials exhibit a broadband spectrum typical of infinite nanowire arrays, although the Au nanoparticles are electrically disconnected. Accordingly, it is possible to design plasmonic nanostructures capable of an efficient harvesting of light either in the visible or in the near infrared regime depending on the polarization of the incident light. The method offers many advantages (applicable to a wide range of materials, possibility to tune the periodicity and the morphology of the aligned nanoparticles by changing the prepatterning and deposition conditions, fast output and low production costs, etc.) that make it attractive for numerous plasmonic applications.

* * *

We would like to acknowledge assistance from SOLEIL staff during the GISAXS experiments at the SWING beamline.

REFERENCES

[1] Maier S. A. and Atwater H. A., *J. Appl. Phys.*, **98** (2005) 011101.
[2] Pillai S., Catchpole K. R., Trupke T. and Green M. A., *J. Appl. Phys.*, **101** (2007) 093105.
[3] Martín J. I., Nogués J., Liu K., Vicent J. L. and Schuller I. K., *J. Magn. & Magn. Mater.*, **256** (2003) 449.
[4] Polman A., *Science*, **322** (2008) 868.
[5] Fort E., Ricolleau C. and Sau-Pueyo J., *Nano Lett.*, **3** (2003) 65.
[6] Haynes C. L. and Van Duyne R. P., *Nano Lett.*, **3** (2003) 939.
[7] Cuccureddu F., Murphy S., Shvets I. V., Porcu M. and Zandbergen H. W., *Nano Lett.*, **8** (2008) 3248.
[8] Gotschy W., Vonmetz K., Leitner A. and Aussenegg F. R., *Opt. Lett.*, **21** (1996) 1099.
[9] Schider G., Krenn J. R., Gotschy W., Lamprecht B., Ditlbacher H., Leitner A. and Aussenegg F. R., *J. Appl. Phys.*, **90** (2001) 3825.
[10] Lu A. H., Lu G. H., Kessinger A. M. and Foss C. A., *J. Phys. Chem. B*, **101** (1997) 9139.
[11] Swami A., Selvakannan P., Pasricha R. and Sastry M., *J. Phys. Chem. B*, **108** (2004) 19269.
[12] Pérez-Juste J., Rodríguez-González B., Mulvaney P. and Liz-Marzán L. M., *Adv. Funct. Mater.*, **15** (2005) 1065.
[13] Liu Q., Cui Y., Gardner D., Li X., He S. and Smalyukh I. I., *Nano Lett.*, **10** (2010) 1347.
[14] Oates T. W. H., Keller A., Facsko S. and Mücklich A., *Plasmonics*, **2** (2007) 47.
[15] Toma A., Chiappe D., Massabo D., Boragno C. and de Mongeot F. B., *Appl. Phys. Lett.* , **93** (2008) 163104.
[16] Camelio S., Babonneau D., Lantiat D., Simonot L. and Pailloux F., *Phys. Rev. B*, **80** (2009) 155434.
[17] Ranjan M., Oates T. W. H., Facsko S. and Möller W., *Opt. Lett.*, **35** (2010) 2576.
[18] Babonneau D., *J. Appl. Crystallogr.*, **43** (2010) 929.
[19] Leroy F., Lazzari R. and Renaud G., *Acta Crystallogr. A*, **60** (2004) 565.
[20] Lazzari R., Renaud G., Revenant C., Jupille J. and Borensztein Y., *Phys. Rev. B*, **79** (2009) 125428.
[21] Camelio S., Babonneau D., Lantiat D. and Simonot L., *EPL*, **79** (2007) 47002.
[22] Toma A., Chiappe D., Boragno C. and Buatier de Mongeot F., *Phys. Rev. B*, **81** (2010) 165436.
[23] Aubry A., Lei D. Y., Maier S. A. and Pendry J. B., *Phys. Rev. B*, **82** (2010) 125430.
[24] Marhaba S., Bachelier G., Bonnet C., Broyer M., Cottancin E., Grillet N., Lerme J., Vialle J.-L. and Pellarin M., *J. Phys. Chem. C*, **113** (2009) 4349.